#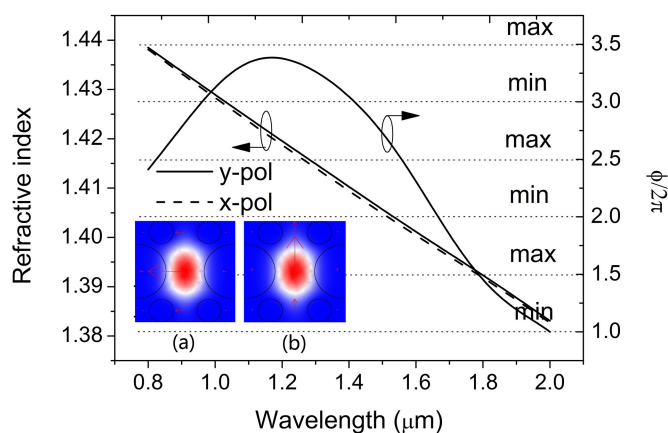 Analysis of a Magnetic Field Sensor Based on a Sagnac Interferometer Using a Magnetic Fluid-Filled Birefringent Photonic Crystal Fiber

Mingjian Ma
Hailiang Chen
Shuguang Li
Xili Jing
Wenxun Zhang
Mingyue Wang

Analysis of a Magnetic Field Sensor Based on a Sagnac Interferometer Using a Magnetic Fluid-Filled Birefringent Photonic Crystal Fiber

Mingjian Ma, Hailiang Chen [ORCID]**, Shuguang Li, Xili Jing, Wenxun Zhang, and Mingyue Wang**

State Key Laboratory of Metastable Materials Science and Technology and Key Laboratory for Microstructural Material Physics of Hebei Province, School of Science, Yanshan University, Qinhuangdao 066004, China

Abstract: A magnetic field sensor based on a Sagnac interferometer using a magnetic fluid-filled birefringent photonic crystal fiber (MF-BPCF) was proposed and studied by finite element method. Two large air holes in the birefringent photonic crystal fiber were designed to fill with magnetic fluid. The MF-BPCF in the proposed Sagnac interferometer acted as the sensing head. As magnetic field perpendicular to the MF-BPCF, magnetic fluid was anisotropic. The characteristics of the output spectrum of the Sagnac interferometer was simulated. The results showed that when the phase difference ϕ satisfied integer multiples of 2π, several dip wavelengths appeared. Not only the intensity but also the direction of the magnetic field was measured. The measuring sensitivity could be further promoted by making the dip wavelength approach $\lambda_{B_g=0}$.

Index Terms: Magnetic field sensor, Photonic crystal fiber, Magnetic fluid, Sagnac interferometer.

1. Introduction

Magnetic fluid (MF) is a single-domain colloidal solution by dispersing nano-scale magnetic particles in liquid carriers with the aid of surfactants [1], [2]. Fe_3O_4, Fe_2O_3, Ni, and Co are the common used magnetic particle materials. The carriers are usually water, kerosene and heptane. The refractive index of the MF is dependent on the magnetic particles and carriers [3], [4]. It increases linearly as the concentration of magnetic particles increase. When the magnetic field is applied on MF, magnetic particles polarize along the direction of the magnetic field and form magnetic chains. As the magnetic field increases, the refractive index of MF increases gradually and finally to a saturated value. Langevin function was used to describe the refractive index of MF as functions of magnetic field and temperature [5], [6]. MF is isotropic when the direction of incident light is parallel to the magnetic chains. MF becomes anisotropic as the direction of incident light is perpendicular

to the magnetic chains. P. C. Scholten investigated the birefringence of MF for the first time [7]. The extraordinary and ordinary refractive indices of MF were deduced in literatures [8], [9].

Owing to the excellent properties such as refractive index tunability, birefringence effect, dichroism effect, magnetochromatics, Faraday effect and field dependent transmission, MF has attracted lots of attentions and has been widely studied in science and technology areas [10], [12]. Dong *et al.* reported a magnetic field sensor by covering MF on a section of tapered and lateral-offset splicing traditional fiber. The sensitivity reached 26 pm/Oe in the range of 250–475 Oe [13]. Xiaoping Li *et al.* made the magnetic field perpendicular to the tapered traditional fiber which was covered by MF. They detected the magnetic field intensity by measuring the polarization degree [14]. H. E. Horng *et al.* designed a modulator by covering MF on a grooved optical fiber. The modulation deep could be higher than 20% by several cascaded modulators [15]. Sagnac interferometer which shows high spectrum sharpness has been used to measure various physical parameters [16], [17]. Zu *et al.* investigated a magnetic field sensor by inserting MF film into a Sagnac interferometer [18]. Since the direction of the magnetic field was perpendicular to the direction of light propagation, MF was anisotropic. The shift of valley wavelength depicted a nonlinear relationship with magnetic field and finally a best sensitivity of 592.8 pm/Oe was achieved. However, the thickness of MF film should be narrower than 100 μm due to the large transmission loss of MF. Meanwhile, the device of MF film-inserting Sagnac interferometer was not robust.

Photonic crystal fiber (PCF) with air holes distributing in the cladding area, supplies channels for the infilling of functional materials [19], [24]. PCF which was filled with MF in the cladding air holes has been used as magnetic field tunable bandgap guiding and modes coupling devices [25], [26]. In these devices, the power of light mainly transmitted in the silica core rather than in the MF columns. It can support a long transmitting distance. The long transmitting distance also enhances the influence of MF on guiding modes. The infilling of MF in the cladding air holes of PCF also improves the robustness. R. Gao *et al.* investigated the variation of output light intensity based on MF partially filled PCF. The magnetic field measuring sensitivity reached 0.011 μW/Oe [27]. Harneet V. Thakur *et al.* studied a polarization interference based on a MF-filled PCF. The magnetic field measuring sensitivity was 24.2 pm/Oe [28].

So far, the anisotropy of MF in MF-filled PCF devices was rarely considered. In this paper, we proposed a magnetic field sensor based on a Sagnac interferometer using a MF-filled birefringent PCF (MF-BPCF). MF was designed to fill into two large air holes in PCF. The two MF columns which were located near the fiber core were benefit to adjust the refractive indices of core guiding modes. The MF-BPCF was then introduced into a Sagnac interferometer and acted as the sensing head. The magnetic field was perpendicular to the PCF axis. Therefore, the MF was anisotropic. Both the intensity and direction of the magnetic field showed influences on the output spectrum of the Sagnac interferometer. The simulation results depicted that several dip wavelengths appeared when the phase difference ϕ satisfied integer multiples of 2π. The influences of magnetic field intensity, magnetic field direction and temperature on dip wavelengths were then investigated. Finally, we analyzed the optimization of magnetic field measuring sensitivity.

2. Design of the Sagnac Interferometer and Operation Principles

Fig. 1(a) shows the schematic of the Sagnac interferometer. The broadband light source (BBS) outputs laser into the 3 dB coupler. The 3 dB coupler splits the laser into two counter propagating waves. Polarization controller (PC) rotates the polarization direction of the incident linearly polarized light by 90°. The MF-BPCF is designed to insert into the Sagnac loop by splicing with two single mode fibers (SMFs). The anticlockwise propagating wave gets through PC first and then the MF-BPCF. On the contrary, the clockwise propagating wave gets through the MF-BPCF first and then the PC. The two counter propagating waves encounter and interfere at the output port of the 3 dB coupler. Optical spectrum analyzer (OSA) is used to measure the transmission spectrum. The
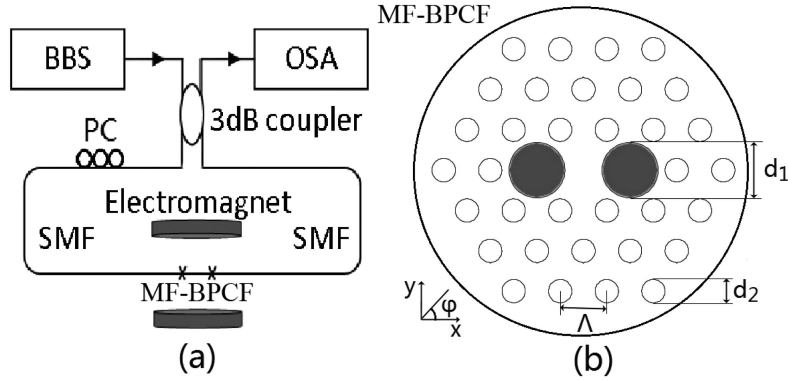
Fig. 1. (a) Schematic of the Sagnac interferometer and (b) cross-section of the MF-BPCF.

normalized intensity of the transmission spectrum can be described as:

$$P = [1 - \cos(\phi)]/2 \tag{1}$$

where the phase difference $\phi = 2\pi BL/\lambda$, B is the mode birefringence in MF-BPCF, L is the length of MF-BPCF, and λ is the wavelength in free space.

Fig. 1(b) depicts the cross-section of the MF-BPCF. The background material of PCF is silica. The cladding air holes are arranged in hexagonal lattice with adjacent air holes pitch of Λ. Two large air holes with diameter of d_1 are located near the PCF core. The rest air holes are of the same diameter of d_2. In order to achieve the function of magnetic field sensing, the two large air holes are designed to fill with MF. The magnetic field which is generated by electromagnets induces the reorientation of magnetic particles along the external magnetic field. φ indicates the direction of magnetic field. Along with the infilling of MF, the mode birefringence of PCF is influenced by magnetic field. The permittivity tensor ε_r of MF is expressed by the following equation,

$$\varepsilon_r = \begin{pmatrix} \varepsilon_\perp \sin^2(\varphi) + \varepsilon_\parallel \cos^2(\varphi) & (\varepsilon_\parallel - \varepsilon_\perp)\cos(\varphi)\sin(\varphi) & 0 \\ (\varepsilon_\parallel - \varepsilon_\perp)\cos(\varphi)\sin(\varphi) & \varepsilon_\perp \cos^2(\varphi) + \varepsilon_\parallel \sin^2(\varphi) & 0 \\ 0 & 0 & \varepsilon_\perp \end{pmatrix} \tag{2}$$

where $\varepsilon_\perp$ and $\varepsilon_\parallel$ represent the permittivities that electrical field of incident light is perpendicular and parallel to the external magnetic field, respectively. $\varepsilon_\perp$ and $\varepsilon_\parallel$ are described in [8],

$$\varepsilon_\parallel = \varepsilon_f + (\varepsilon_p - \varepsilon_f)\varphi_m\beta \left[1 + \frac{4\pi}{3}\varphi_m\alpha(1 + 0.8\eta L^2(\kappa)) \right]$$

$$\varepsilon_\perp = \varepsilon_f + (\varepsilon_p - \varepsilon_f)\varphi_m\beta \left[1 + \frac{4\pi}{3}\varphi_m\alpha(1 - 0.4\eta L^2(\kappa)) \right] \tag{3}$$

where ε_f is the permittivity of liquid carrier, ε_p is the permittivity of magnetic particles, φ_m is the magnetic particles concentration, $\beta = \frac{3\varepsilon_f}{2\varepsilon_f + \varepsilon_p}$, $\alpha = \frac{3}{4\pi}\frac{\varepsilon_p - \varepsilon_f}{2\varepsilon_f + \varepsilon_p}$, $\eta = \frac{\mu_0}{4\pi}\frac{m^2}{d_h^3 k_B T}$, $k = \mu_0 \frac{mH}{k_B T}$, and $L(k) = \coth(k) - 1/k$. μ_0 is the magnetic permeability of vacuum. m is the magnetic moment of magnetic particle. d_h is the magnetic particle diameter. k_B is Boltzmann constant. T is temperature in Kelvin. H is the magnetic field. In this study, Fe_3O_4 and water were designed as the magnetic particle and solvent respectively. The complex permittivity of Fe_3O_4 and water as a function of wavelength can be referred in [29], [30].

Fig. 2 shows the complex permittivity of MF as a function of magnetic field. The wavelength and temperature were set as 1.3 μm and 300 K respectively. Both the real and imaginary part of the permittivity of $\varepsilon_\parallel$ and $\varepsilon_\perp$ showed different variation tendency. As magnetic field increased, $Re(\varepsilon_\parallel)$
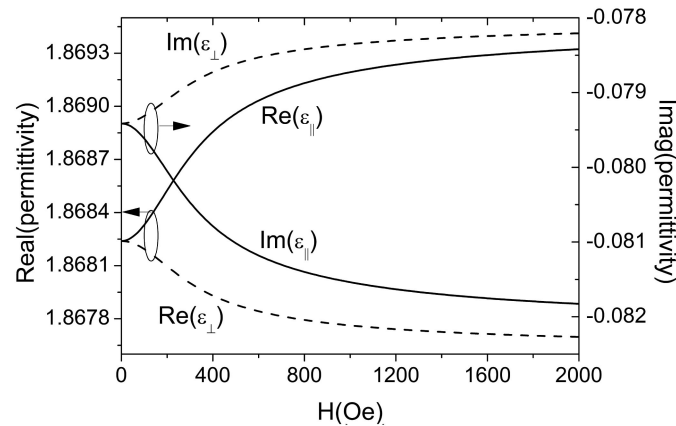
Fig. 2. Complex permittivity of MF as a function of magnetic field.

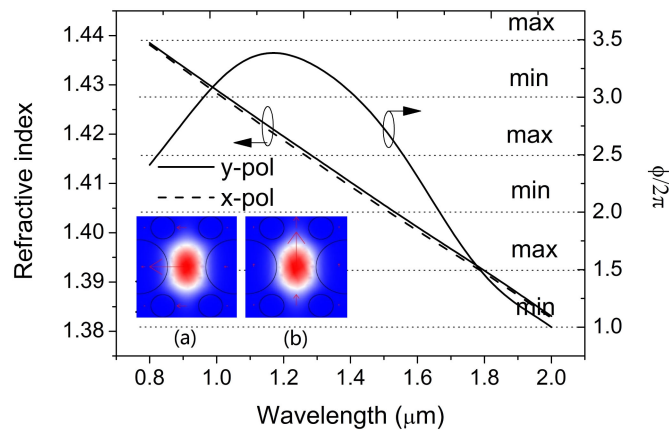Fig. 3. Refractive indices of core fundamental modes and $\phi/2\pi$ as a function of wavelength. The parameters were set as $d_1 = 2.4$ μm, $d_2 = 1.0$ μm, $\Lambda = 2.0$ μm, $L = 5$ mm, $\varphi = 90°$, T = 300 K, and H = 100 Oe. Insets (a) and (b) show the electrical field distributions of core fundamental modes in x-polarized direction and y-polarized direction, respectively.

increased to a saturation value while Re($\varepsilon_\perp$) decreased to a saturation value. The imaginary part of the permittivity depicted an inverse situation.

3. Sensing Characteristics of the Designed Sagnac Interferometer

The model features of the MF-BPCF were simulated by using COMSOL software. First, a perfect matched layer (PML) was added on the outside of the MF-BPCF. Second, the different areas of the MF-BPCF were attributed with corresponding optical constants. Third, the cross-section of the MF-BPCF was divided into about 8826 triangular meshes. Fourth, the complex propagating constants of eigenmodes were calculated based on the Helmholtz equation and scattering boundary condition. The other parameters such as refractive index, birefringence and confinement loss were deduced. Fig. 3 shows the refractive indices of core fundamental modes and $\phi/2\pi$ as a function of wavelength. The parameters were set as $d_1 = 2.4$ μm, $d_2 = 1.0$ μm, $\Lambda = 2.0$ μm, $L = 5$ mm, $\varphi = 90°$, T = 300 K, and H = 100 Oe. The electrical field distributions of core fundamental modes in x-polarized direction and y-polarized direction are shown in insets (a) and (b) respectively. As wavelength increased from 0.8 to 2.0 μm, the refractive indices of the two orthogonally polarized core modes decreased. However, the mode birefringence B increased at first and then decreased, owing to
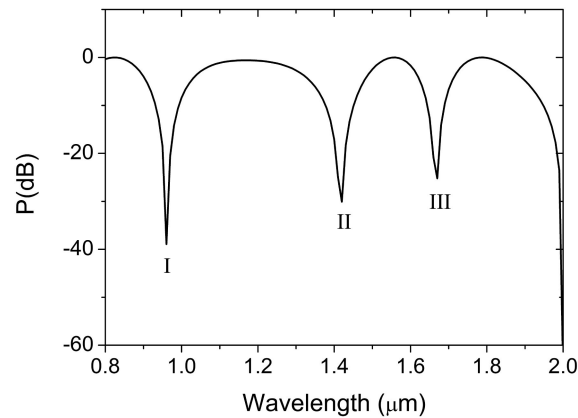
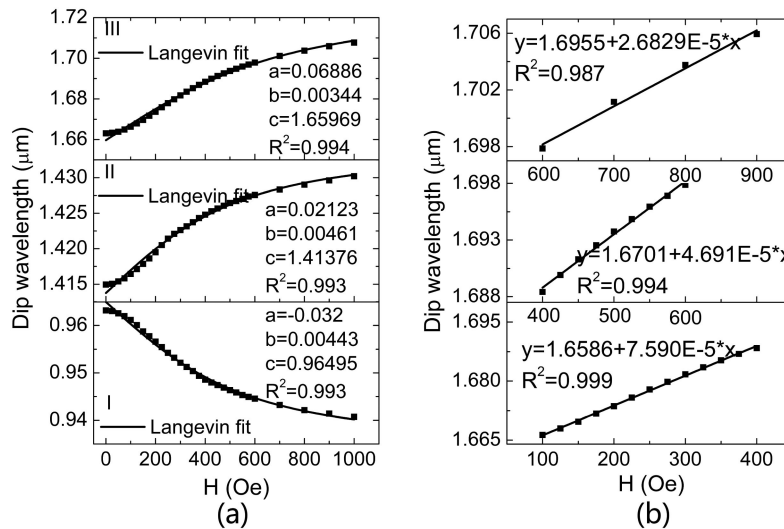Fig. 4. Normalized output power *P* (in dB) as a function of wavelength.

Fig. 5. Dip wavelength as a function of magnetic field. (a) Langevin function fitting for valleys I, II and III. (b) Linear fitting for valley III.

the asymmetric structure in MF-BPCF and confinement effect of mode field in core area. Phase difference ϕ showed similar variation tendency with B. On the one hand, when ϕ satisfied integer multiples of 2π, the normalized output power of the Sagnac interferometer reached the minimum value. On the other hand, when ϕ satisfied half integer multiples of 2π, the normalized output power reached the maximum value as shown in Eqs. (4).

Fig. 4 depicts the normalized output power P (in dB) as a function of wavelength. Three valleys appeared and were labeled by I, II and III. Valleys I and II were corresponding to $\phi = 6\pi$ while valley III was corresponding to $\phi = 4\pi$. Because the permittivity of MF was influenced by magnetic field, the refractive indices of core fundamental modes in MF-BPCF changed and as a result the spectrum of the Sagnac interferometer shifted when magnetic field varied. As magnetic field increased, the refractive index of core fundamental mode in x-polarized direction decreased while that in y-polarized direction increased. Therefore, the mode birefringence B and phase difference ϕ increased.

The dip wavelength at valley I, II and III as a function of magnetic field are shown in Fig. 5(a). As magnetic field increased, valley I experienced a blue shift contrast to the red shifts for valley II and III.
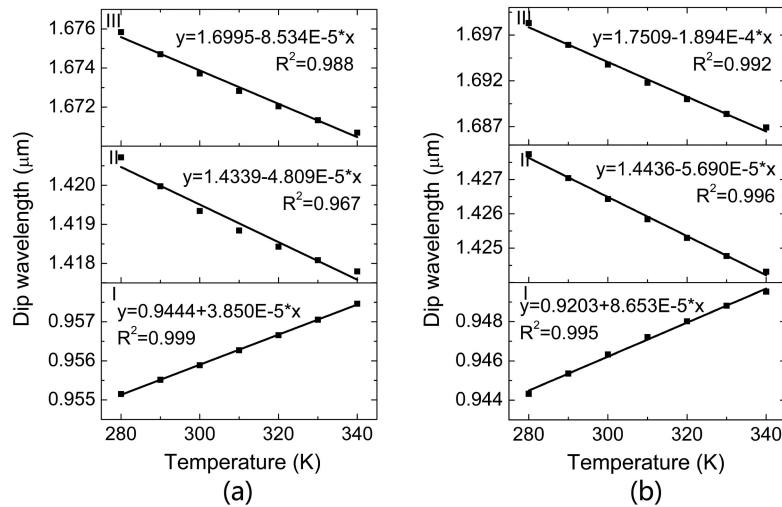
Fig. 6. Dip wavelength in valley I, II and III as a function of temperature. (a) H = 200 Oe, (b) H = 500 Oe.

Langevin function was used to fit the curves as shown in Fig. 5(a). Langevin function was set as

$$y = a \left[\coth(bx) - \frac{1}{bx} \right] + c. \tag{4}$$

It can be seen from Fig. 5(a) that Langevin function depicted a good fitting at higher magnetic field. It is benefit for practical use when the dip wavelength shows a linear relationship with magnetic field. Thus, we divided the whole scale of magnetic field into several short ranges and fit the data with straight lines. Fig. 5(b) shows the linear fitting for valley III. The straight lines depicted a good fitting for the magnetic field range of 100–400 Oe and 400–600 Oe. The linear fitting got worse as the magnetization of MF tended to saturation. The measuring sensitivity of magnetic field reached 7.59E-5, 4.69E-5 and 2.68E-5 μm/Oe in the magnetic field range of 100–400 Oe, 400-600 Oe and 600–1000 Oe.

The reorientation of magnetic particles in MF along external magnetic field is also influenced by the thermal effect. As temperature increases, the thermal energy of magnetic particles increases which prevents the reorientation. As a result, The variation trend of MF permittivity depending on temperature is opposite to magnetic field. The output spectrum of the designed Sagnac interferometer was then affected by the temperature. The dip wavelength in valleys I, II and III variation with temperature are shown in Fig. 6. As temperature increased, the dip wavelength increased in valley I while decreased in valley II and III. This was owing to the decrease of B. The dip wavelength exhibited a linear relationship with temperature in the range of 280-340 K. Valley III depicted a relative higher sensitivity than valley I and II. The temperature sensitivity was 3.850E-5, −4.809E-5 and −8.534E-5 μm/K for valleys I, II and III respectively at $H = 200$ Oe. As the magnetic field was 500 Oe, the temperature sensitivity increased to 8.653E-5, −5.690E-5 and −1.894E-4 μm/K for valleys I, II and III correspondingly.

The magnetic moment of magnetic chains in MF reorients along the external magnetic field when the angle φ of magnetic field changes. The refractive indices of the two orthogonally polarized modes in MF-BPCF alter accordingly which finally results in the shift of the output spectrum in Sagnac interferometer. Fig. 7(a) shows the dip wavelength in valleys I, II and III as a function of magnetic field at different magnetic field rotation angle of φ. As $\varphi = 0°$, the refractive index of MF in x-polarized direction was bigger than in y-polarized direction. As a result, B decreased and the dip wavelength increased for valley I and decreased for valley II and III when the magnetic field increased. The opposite was true when $\varphi = 90°$. As wavelength increased, the mode area increased
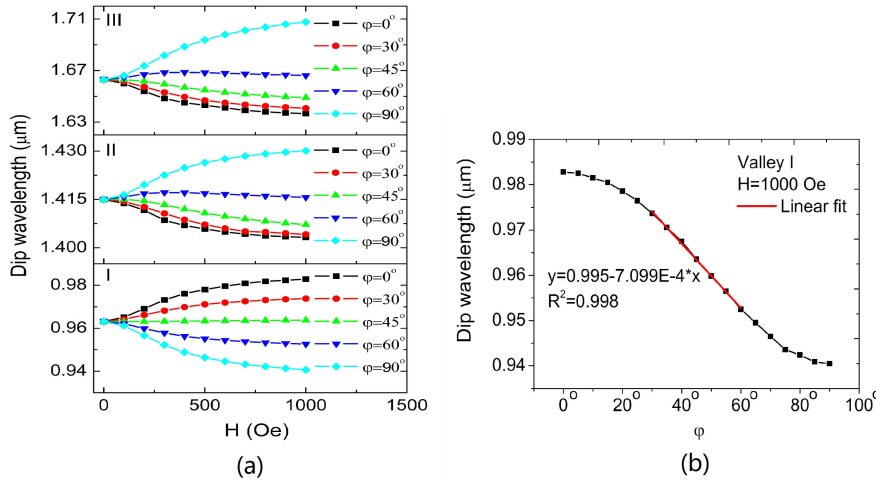
Fig. 7. (a) Dip wavelength in valley I, II and III as a function of magnetic field at different magnetic field rotation angle of φ. (b) Dip wavelength in valley I as a function of rotation angle φ at H = 1000 Oe. Temperature was set as 300 K.

and the influences of asymmetric distribution in MF-BPCF on B increased for both valley II and III. The variation velocity of dip wavelength as a function of φ increased gradually at lower magnetic field and saturated at higher magnetic field. Fig. 7(b) shows the dip wavelength as a function of rotation angle φ for valley I at H = 1000 Oe. As φ increased from 0° to 90°, the dip wavelength gradually decreased. The decrease velocity was slower as φ approached 0° and 90° while became faster as φ approached 45°. Linear fitting was carried out in the range of 30° to 60°. The angle measurement sensitivity reached 7.099E-4 μm/degree in this range.

4. Optimization of the Sensitivity

The dip wavelength in the output spectrum of the Sagnac interferometer appears as ϕ satisfying the following formula:

$$\phi = 2\pi B L / \lambda = 2\pi m \tag{5}$$

where m is an integer. The birefringence B and wavelength λ depend on the magnetic field H. By taking the derivative of the both sides of Eqs. (5) and substituting the formula $\frac{\partial B}{\partial H} = \frac{\partial B}{\partial \lambda} \mid_H \times \frac{\partial \lambda}{\partial H} + \frac{\partial B}{\partial H} \mid_\lambda$, the sensitivity S was obtained,

$$S = \frac{\partial \lambda}{\partial H} = \frac{\lambda \frac{\partial B}{\partial H} \mid_\lambda}{B_g} = \frac{\lambda \frac{\partial B}{\partial H} \mid_\lambda}{B - \lambda \frac{\partial B}{\partial \lambda} \mid_H} \tag{6}$$

where the group birefringence $B_g = B - \lambda \frac{\partial B}{\partial \lambda} \mid_H$. Fig. 8(a) shows the $\partial B / \partial H$ as a function of magnetic field. λ increased from 1.10 to 1.19 μm in a step of 0.01 μm. As magnetic field increased, $\partial B / \partial H$ increased at first and then decreased to a constant value. $\partial B / \partial H$ experienced a small change as wavelength varied. Fig. 8(b) depicts the group birefringence B_g as a function of wavelength. The magnetic field H increased from 0 to 1000 Oe in a step of 100 Oe. As magnetic field increased, B_g showed a minor variation at short wavelength while depicted a relative larger variation at long wavelength. B_g reached zero at a certain wavelength. Inset in Fig. 8(b) exhibits the enlarged image with B_g close to zero. The wavelength at $B_g = 0$ ($\lambda_{B_g=0}$) showed a minor reduction as magnetic field increased. The value of B_g is negative when wavelength is smaller than $\lambda_{B_g=0}$ and positive when wavelength is bigger than $\lambda_{B_g=0}$. The magnetic field measuring sensitivity S is in direct proportion to $\partial B / \partial H$ and inverse proportion to B_g. Therefore, we can promote the sensitivity by increasing $\partial B / \partial H$ or reducing the absolute value of B_g.
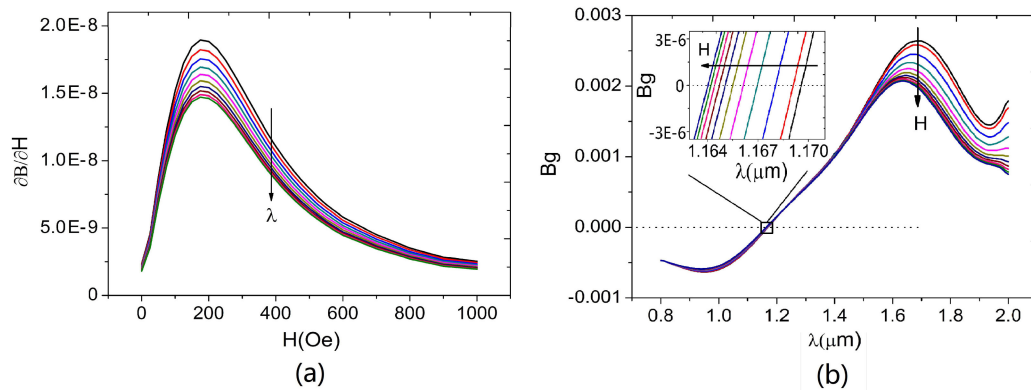
Fig. 8. (a) $\partial B/\partial H$ as a function of magnetic field. The wavelength λ increases from 1.10 to 1.19 μm in a step of 0.01 μm. (b) Group birefringence B_g as a function of wavelength. The magnetic field H increases from 0 to 1000 Oe in a step of 100 Oe. Inset in (b) is the enlarged image with B_g close to zero.
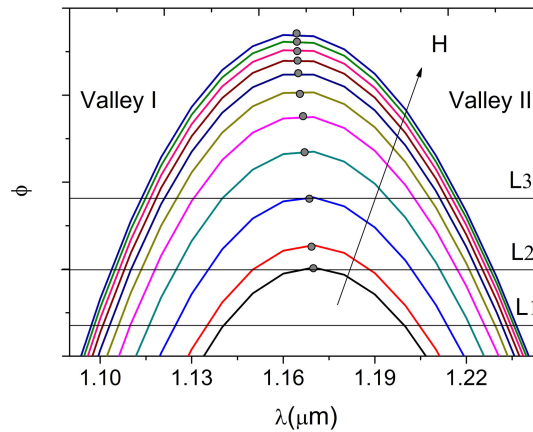

Fig. 9. (a) Phase difference ϕ as a function of wavelength. The magnetic field H increases from 0 to 1000 Oe in a step of 100 Oe. Grey circles represent $\lambda_{B_g=0}$ at different magnetic fields.

The PCF structure parameters such as d_1, d_2 and Λ, could be used to adjust the characteristics of eigenmodes. However, the relationship between these parameters and refractive indices of eigenmodes are usually complicated. In the designed Sagnac interferometer, phase difference ϕ showed a linear relationship with PCF length L. Therefore, we can conveniently tune the dip wavelength by changing the MF-BPCF length. Fig. 9 depicts the phase difference ϕ as a function of wavelength. The magnetic field H increases from 0 to 1000 Oe in a step of 100 Oe. Grey circles represent $\lambda_{B_g=0}$ at different magnetic fields. Three horizontal lines on behalf of three PCF lengths of $L1$, $L2$ and $L3$ are drawn in Fig. 9. The abscissa of the intersection points between these horizontal lines and $\phi(\lambda)$ represents the dip wavelengths. As the MF-BPCF length is set as $L2$, the horizontal line gets through the point of $\lambda_{B_g=0}$ at $H = 0$ Oe. As magnetic field decreased, the dip wavelength increased in valley I and decreased in valley II. The magnetic field measuring sensitivity reached infinity at $H = 0$ Oe in theory. As the MF-BPCF length increased to $L1$, the intersection points moved downward. The dip wavelength could be separated clearly by valley I and II. Meanwhile, the magnetic field measuring sensitivity decreased. As L decreased to $L3$, the intersection points moved upward. The magnetic field measuring sensitivity reached infinity at $H = 200$ Oe in theory. The above analysis shows us a way how to promote the sensitivity.
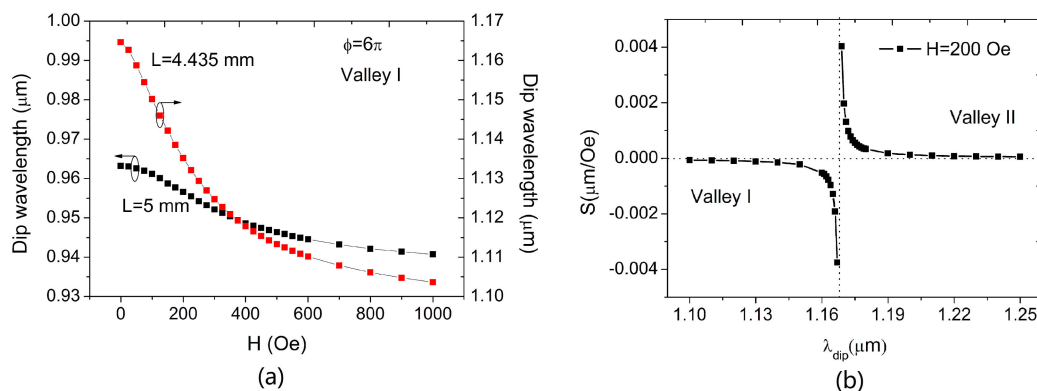
Fig. 10. (a) Dip wavelength in valley I as a function of magnetic field. The MF-BPCF length is 4.435 and 5 mm respectively. The phase difference $\phi = 6\pi$. (b) Magnetic field measuring sensitivity as a function of λ_{dip} at H = 200 Oe.

Fig. 10(a) shows the dip wavelength in valley I as a function of magnetic field. The PCF length is 4.435 and 5 mm respectively. The phase difference $\phi = 6\pi$. The temperature was set as 300 K. Contrast to $L = 5$ mm, $L = 4.435$ mm is more approaching $L2$. It can be seen that the dip wavelength experiences a faster shift at $L = 4.435$ mm than at $L = 5$ mm. The sensitivity at $L = 4.435$ mm is several times higher than at $L = 5$ mm. For instance, the sensitivity at H = 100 Oe is $-11.70E-4$ μm/Oe for $L = 4.435$ mm and $-3.86E-5$ μm/Oe for $L = 5$ mm. Fig. 10(b) depicts the magnetic field measuring sensitivity as a function of λ_{dip} at H = 200 Oe. $\lambda_{B_g=0}$ is 1.168 μm for H = 200 Oe. As the dip wavelength is close to 1.168 μm, the absolute value of sensitivity increases obviously in both valley I and II. The sensitivity reaches an infinite at $\lambda_{B_g=0}$ in theory. The sensitivity at other values of magnetic field could also be promoted greatly through tuning the dip wavelength to the corresponding $\lambda_{B_g=0}$ by just changing the MF-BPCF length.

5. Conclusion

In this paper, a magnetic field sensor based on a Sagnac interferometer using a MF-BPCF was proposed and investigated by finite element method. Because the direction of magnetic field was perpendicular to the MF-BPCF, MF was anisotropic for the incident light. The simulation results showed that several dip wavelengths appeared as phase difference ϕ satisfied integer multiples of 2π. The magnetic field intensity, temperature and magnetic field direction were detected based on their influences on the permittivity of MF. Langevin function was used to fit the relationship between magnetic field intensity and dip wavelength in the whole range. Linear fitting was implemented in several short ranges. Contrast to magnetic field, temperature depicted an opposite effect on the shift of dip wavelength. The relationship between the magnetic field direction and dip wavelength was also studied. At last, we analyzed the optimization of magnetic field measuring sensitivity. By adjusting the MF-BPCF length to make the dip wavelength close to $\lambda_{B_g=0}$, the sensitivity could be promoted greatly. The analysis method in this paper provides a reference for other interferometer-based sensors.

References

[1] B. M. Lacava *et al.*, "Particle sizing of magnetite-based magnetic fluid using atomic force microscopy: A comparative study with electron microscopy and birefringence," *Appl. Phys. Lett.*, vol. 77, pp. 1876–1878, 2000.
[2] P. C. Morais, K. S. Neto, A. F. Bakuzis, M. F. Da Silva, and N. Buske, "Birefringence of magnetite-based magnetic fluids: The effect of the surface-coating layer," *IEEE Trans. Magn.*, vol. 38, no. 5, pp. 3228–3230, Sep. 2002.
[3] C. Y. Hong, H. E. Horng, and S. Y. Yang, "Tunable refractive index of magnetic fluids and its applications," *Phys. Status Solidi (c)*, vol. 1, pp. 1604–1609, 2004.

[4] Y. Zhao, D. Wu, R. Q. Lv, and Y. Ying, "Tunable characteristics and mechanism analysis of the magnetic fluid refractive index with applied magnetic field," *IEEE Trans. Magn.*, vol. 50, no. 8, pp. 1–5, Aug. 2014.

[5] Y. F. Chen, S. Y. Yang, W. S. Tse, H. E. Horng, C. Y. Hong, and H. C. Yang, "Thermal effect on the field-dependent refractive index of the magnetic fluid film," *Appl. Phys. Lett.*, vol. 82, pp. 3481–3483, 2003.

[6] L. X. Chen, X. G. Huang, J. H. Zhu, G. C. Li, and S. Lan, "Fiber magnetic-field sensor based on nanoparticle magnetic fluid and Fresnel reflection," *Opt. Lett.*, vol. 36, pp. 2761–2763, 2011.

[7] P. C. Scholten, "The origin of magnetic birefringence and dichroism in magnetic fluids," *IEEE Trans. Magn.*, vol. MAG-16, no. 2, pp. 221–225, Mar. 1980.

[8] A. Y. Zubarev, "On the theory of birefringence in magnetic fluids," *Colloid J.*, vol. 74, pp. 695–702, 2012.

[9] S. Taketomi, S. Ogawa, H. Miyajima, and S. Chikazumi, "Magnetic birefringence and dichroism in magnetic fluid," *IEEE Transl. J. Magn. Jpn.*, vol. 4, no. 6, pp. 384–394, Jun. 1989.

[10] M. P. Pileni, "Magnetic fluids: Fabrication, magnetic properties, and organization of nanocrystals," *Adv. Funct. Mater.*, vol. 11, pp. 323–336, 2001.

[11] A. Jordan, R. Scholz, P. Wust, H. Fahling, and R. Felix, "Magnetic fluid hyperthermia (MFH): Cancer treatment with AC magnetic field induced excitation of biocompatible superparamagnetic nanoparticles," *J. Magn. Magn. Mater.*, vol. 201, pp. 413–419, 1999.

[12] J. Zheng *et al.*, "Magnetic field sensor using tilted fiber grating interacting with magnetic fluid," *Opt. Exp.*, vol. 21, pp. 17863–17868, 2013.

[13] S. Dong, S. Pu, and H. Wang, "Magnetic field sensing based on magnetic-fluid-clad fiber-optic structure with taper-like and lateral-offset fusion splicing," *Opt. Exp.*, vol. 22, pp. 19108–19116, 2014.

[14] X. Li, R. Ma, and Y. Xia, "Magnetic field sensor exploiting light polarization modulation of microfiber with magnetic fluid," *J. Lightw. Technol.*, vol. 36, no. 9, pp. 1620–1625, May 2018.

[15] H. E. Horng, J. J. Chieh, Y. H. Chao, S. Y. Yang, C.-Y. Hong, and H. C. Yang, "Designing optical-fiber modulators by using magnetic fluids," *Opt. Lett.*, vol. 30, pp. 543–545, 2005.

[16] D. H. Kim and J. U. Kang, "Sagnac loop interferometer based on polarization maintaining photonic crystal fiber with reduced temperature sensitivity," *Opt. Exp.*, vol. 12, pp. 4490–4495, 2004.

[17] X. Dong, H. Y. Tam, and P. Shum, "Temperature-insensitive strain sensor with polarization-maintaining photonic crystal fiber based Sagnac interferometer," *Appl. Phys. Lett.*, vol. 90, 2007, Art. no. 151113.

[18] P. Zu *et al.*, "Enhancement of the sensitivity of magneto-optical fiber sensor by magnifying the birefringence of magnetic fluid film with Loyt-Sagnac interferometer," *Sens. Actuators B, Chem.*, vol. 191, pp. 19–23, 2014.

[19] S. Weng, L. Pei, J. Wang, T. Ning, and J. Li, "High sensitivity D-shaped hole fiber temperature sensor based on surface plasmon resonance with liquid filling," *Photon. Res.*, vol. 5, pp. 103–107, 2017.

[20] C. Lin *et al.*, "Liquid modified photonic crystal fiber for simultaneous temperature and strain measurement," *Photon. Res.*, vol. 5, pp. 129–133, 2017.

[21] H. L. Chen, S. G. Li, Z. K. Fan, G. W. An, J. S. Li, and Y. Han, "A novel polarization splitter based on dual-core photonic crystal fiber with a liquid crystal modulation core," *IEEE Photon. J.*, vol. 6, no. 4, Aug. 2014, Art. no. 2201109.

[22] W. Chen, S. Lou, L. Wang, S. Feng, W. Lu, and S. Jian, "In-fiber modal interferometer based on dual-concentric-core photonic crystal fiber and its strain, temperature and refractive index characteristics," *Opt. Commun.*, vol. 284, pp. 2829–2834, 2011.

[23] M. S. Islam *et al.*, "Localized surface plasmon resonance biosensor: An improved technique for SERS response intensification," *Opt. Lett.*, vol. 44, pp. 1134–1137, 2019.

[24] M. S. Islam *et al.*, "Dual-polarized highly sensitive plasmonic sensor in the visible to near-IR spectrum," *Opt. Exp.*, vol. 26, pp. 30347–30361, 2018.

[25] P. Zu, C. C. Chiu, T. Gong, Y. Jin, W. W. Chang, and X. Y. Dong, "Magneto-optical fiber sensor based on bandgap effect of photonic crystal fiber infiltrated with magnetic fluid," *Appl. Phys. Lett.*, vol. 101, 2012, Art. no. 241118.

[26] H. Chen, S. Li, J. Li, and Z. Fan, "Magnetic field sensor based on magnetic fluid selectively infilling photonic crystal fibers," *IEEE Photon. Technol. Lett.*, vol. 27, no. 7, pp. 717–720, Apr. 2015.

[27] R. Gao, Y. Jiang, and S. Abdelaziz, "All-fiber magnetic field sensors based on magnetic fluid-filled photonic crystal fibers," *Opt. Lett.*, vol. 38, pp. 1539–1541, 2013.

[28] H. V. Thakur, S. M. Nalawade, S. Gupta, R. Kitture, and S. N. Kale, "Photonic crystal fiber injected with Fe_3O_4 nanofluid for magnetic field detection," *Appl. Phys. Lett.*, vol. 99, 2011, Art. no. 161101.

[29] A. Schlegel, S. F. Alvarado, and P. Wachter, "Optical properties of magnetite (Fe_3O_4)," *J. Phys. C, Solid State Phys.*, vol. 12, pp. 1157–1164, 1979.

[30] G. M. Hale and M. R. Querry, "Optical constants of water in the 200-nm to 200-m wavelength region," *Appl. Opt.*, vol. 12, pp. 555–563, 1973.